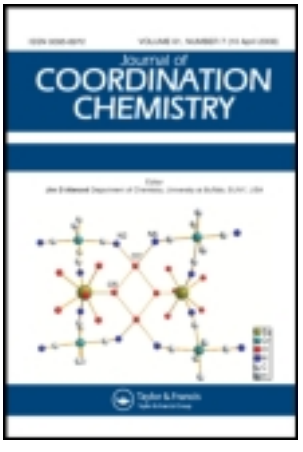

Journal of Coordination Chemistry
Publication details, including instructions for authors and subscription information:
http://www.tandfonline.com/loi/gcoo20

Synthesis, structure, and properties of a 1-D cerium based on monovacant Keggin-type polyoxotungstate

Chao Zhang [a], Pengtao Ma [a], Huanni Chen [a], Jingping Wang [a] & Jingyang Niu [a]

[a] Institute of Molecular and Crystal Engineering, School of Chemistry and Chemical Engineering, Henan University, Kaifeng 475004, P.R. China

Published online: 01 Jul 2011.

To cite this article: Chao Zhang, Pengtao Ma, Huanni Chen, Jingping Wang & Jingyang Niu (2011) Synthesis, structure, and properties of a 1-D cerium based on monovacant Keggin-type polyoxotungstate, Journal of Coordination Chemistry, 64:12, 2178-2185, DOI: 10.1080/00958972.2011.591929

To link to this article: http://dx.doi.org/10.1080/00958972.2011.591929

Journal of Coordination Chemistry
Vol. 64, No. 12, 20 June 2011, 2178–2185

Synthesis, structure, and properties of a 1-D cerium based on monovacant Keggin-type polyoxotungstate

CHAO ZHANG, PENGTAO MA, HUANNI CHEN, JINGPING WANG* and JINGYANG NIU

Institute of Molecular and Crystal Engineering, School of Chemistry and Chemical Engineering, Henan University, Kaifeng 475004, P.R. China

(*Received 18 January 2011; in final form 2 May 2011*)

A new lanthanide-substituted polyoxometalate $[(\alpha\text{-}PW_{11}O_{39})Ce(H_2O)_2]^{4-}$ (**1**) has been synthesized in aqueous solution and characterized by elemental analysis, IR spectrum, UV spectroscopy, thermogravimetric analysis, X-ray powder diffraction (XRPD), and single-crystal X-ray diffraction. The structural analysis reveals that **1** consists of monovacant Keggin-type polyoxoanions $[\alpha\text{-}PW_{11}O_{39}]^{7-}$ as the fundamental building blocks and four $[(CH_3)_4N]^+$ cations. Compound **1** exhibits a 1-D zigzag chain built by $[(\alpha\text{-}PW_{11}O_{39})Ce(H_2O)_2]^{4-}$ moieties. The electrochemical properties of **1** were investigated by cyclic voltammetry in aqueous solution with 0.5 mol L^{-1} Na_2SO_4 as the supporting electrolyte. Magnetic measurements reveal that **1** demonstrates spin–orbital coupling interactions and weak antiferromagnetic exchange interactions.

Keywords: Lanthanide substituted; Polyoxotungstate; Monovacant Keggin-type

1. Introduction

The design, synthesis, and exploitation of lanthanide (Ln)-substituted polyoxometalates (POMs) are driven by their structural diversities, excellent electronic characteristics, and potential applications in the areas of material science, medicine, catalysis, photochemistry, electrochemistry, and magnetism [1–4]. Compared with 3 d-transition-metal cations, Ln cations have stronger oxophilicity, higher coordination numbers, and more flexible coordination geometry. Therefore, the design and synthesis of Ln-substituted POMs with magnetic and other properties are extremely important. In 1971, Peacock and Weakley [5] reported that the reaction of Ln cations and monovacant Keggin polyoxoanions $[XW_{11}O_{39}]^{n-}$ ($X = Si^{IV}$, P^{V}) leads to 1 : 1 and 1 : 2 derivatives. From then on, studies on syntheses of Ln-substituted heteropolytungstates (HPTs) by the reaction of Ln cations and POM precursors derived from Keggin-type polyoxoanions have been well-developed [6, 7]. In the past several years, our group has constructed Ln-substituted POMs derivatives. In this article, we report a 1-D chain-like Ln-substituted

*Corresponding authors. Email: jpwang@henu.edu.cn;jyniu@henu.edu.cn

ISSN 0095-8972 print/ISSN 1029-0389 online
DOI: 10.1080/00958972.2011.591929

phosphotungstate $[(CH_3)_4N]_4[(\alpha\text{-}PW_{11}O_{39})Ce(H_2O)_2]\cdot 2H_2O$ (**1**), which consists of the monovacant Keggin-type building units $[\alpha\text{-}PW_{11}O_{39}]^{7-}$ linked by $[Ce(H_2O)_2]^{3+}$ cations into a 1-D zigzag chain with $[(CH_3)_4N]^+$ as the countercations. The electrochemical properties of **1** were investigated by cyclic voltammetry (CV) in aqueous solution with 0.5 mol L^{-1} Na_2SO_4 as the supporting electrolyte. Magnetic measurements reveal that **1** demonstrates spin–orbital coupling interactions and weak antiferromagnetic exchange interactions.

2. Experimental

2.1. *Instruments and materials*

$Na_7[\alpha\text{-}PW_{11}O_{39}]\cdot nH_2O$ was prepared as described and confirmed by IR spectrum [8]. Other reagents were used as commercially purchased without purification. Elemental analyses (C, H, and N) were conducted on a Perkin-Elmer 2400-II CHNS/O Analyzer; IR spectra were obtained in KBr pellets with a Nicolet FT-IR 360 spectrometer from 4000 to 400 cm^{-1}; X-ray powder diffraction (XRPD) measurements were performed on a Philips X'Pert-MPD instrument with Cu-Kα radiation ($\lambda = 1.54056$ Å) from $2\theta =$ 10–40° at 296(2) K. Thermogravimetric analyses were performed under N_2 on a Mettler-Toledo TGA/SDTA851^e instrument with a heating rate of 10°C min^{-1} from 25°C to 600°C. UV spectrum was recorded on a HITACHI U-4100 UV-Vis-NIR spectrometer (distilled water as solvent) from 400 to 190 nm at 300 K; cyclic voltammetric measurements were performed on a LK98 microcomputer-based electrochemical system (LANLIKE, Tianjin), pH was adjusted with 0.1 mol L^{-1} H_2SO_4 and 0.1 mol L^{-1} NaOH aqueous solution, respectively. Magnetic susceptibility measurements were obtained on a Quantum Design MPMS-XL7 SQUID magnetometer from 2 to 300 K.

2.2. *Preparation of $[(CH_3)_4N]_4[(\alpha\text{-}PW_{11}O_{39})Ce(H_2O)_2]\cdot 2H_2O$ (1)*

$Na_7[\alpha\text{-}PW_{11}O_{39}]\cdot nH_2O$ (2.10 g, 0.73 mmol) was dissolved in 15 mL distilled water at 80°C, followed by dropwise addition of $Ce(NO_3)_3\cdot 6H_2O$ (0.60 g, 1.38 mmol) in 15 mL water. The resulting mixture was adjusted with NaOH to pH = 4.8 under stirring. After 1 h, the mixture was cooled to room temperature and the precipitate was removed by filtration. Then tetramethylammonium bromide (0.20 g, 1.30 mmol) was added. After 30 min, the resulting clear solution was filtered and left to evaporate at room temperature. Brown-yellow crystals of **1** were obtained after 2 weeks (yield: *ca* 30% based on W). IR (KBr pellet): 1630 (m), 1471 (s), 1396 (m), 1079 (s), 980 (s), 897 (s), 814 (s), 595 (w), 519 (m). Anal. Calcd (%): C, 6.03; H, 1.77; N, 1.76. Found (%): C, 5.93; H, 1.98; N, 1.67.

2.3. *X-ray structure determination*

Suitable single crystal of **1** was carefully selected under an optical microscope and attached to the end of a glass fiber with enamel adhesive. X-ray diffraction data were

collected on a Bruker CCD Apex-II diffractometer using Mo-Kα monochromated radiation ($\lambda = 0.71073$ Å) at 296(2) K. The structure was solved by direct methods and refined by full-matrix least-squares on F^2 using *SHELXTL*-97 software [9]. Intensity data were corrected for Lorentz and polarization effects as well as for multi-scan absorption. All non-hydrogen atoms were refined anisotropically. Hydrogens connected to carbon and nitrogen were geometrically placed and not included in the refinements. The summary of crystal data and structure refinements for **1** is listed in table 1. Selected bond lengths are given in table 2.

3. Results and discussion

3.1. *XRPD pattern*

The phase purity of **1** was confirmed by the comparison of its experimental XRPD pattern with the simulated one based on the results from single-crystal X-ray diffraction (figure 1). On account of variation in preferred orientation of the powder sample during collection of the experimental XRPD, the intensity of the experimental and simulated XRPD patterns are different.

3.2. *Crystal structure*

Single-crystal diffraction analysis indicates that **1** crystallizes in the monoclinic $P2(1)/c$ space group, with one mono-Ce^{III}-substituted phosphotungstate anion $[(\alpha\text{-}PW_{11}O_{39})Ce(H_2O)_2]^{4-}$ (figure 2a), four $[(CH_3)_4N]^+$ countercations and two water molecules. Monovacant Keggin-type $[\alpha\text{-}PW_{11}O_{39}]^{7-}$ can be viewed as removal of a WO_t group from the saturated Keggin $[\alpha\text{-}PW_{12}O_{40}]^{3-}$. In the skeleton of **1**, $Ce1^+$ incorporates into the

Table 1. The data collection and refinement parameters of **1**.

Parameter	Value
Empirical formula	$C_{16}H_{56}CeN_4O_{43}PW_{11}$
Space group	$P2(1)/c$
Crystal system	Monoclinic
Unit cell dimensions (Å, °)	
a	12.9063(4)
b	21.9361(7)
c	19.5841(6)
β	90.0680(10)
Z	4
Volume (Å^3)	5544.5(3)
Calculated density (g cm^{-3})	3.817
Absorption coefficient, μ (mm^{-1})	23.649
Limiting indices	$-15 \le h \le 14$; $-23 \le k \le 26$; $-21 \le l \le 23$
Goodness-of-fit on F^2	1.007
R_1[a]	0.0427
wR_2[b]	0.0772

[a] $R_1 = \Sigma\|F_o|-|F_c\|/\Sigma|F_o|$; [b] $wR_2 = [\Sigma w(F_o^2 - F_c^2)^2/\Sigma w(F_o^2)^2]^{1/2}$.

Table 2. Selected bond lengths (Å) for **1**.

Bond	*D* (Å)
Ce(1)–O(16)	2.396(8)
Ce(1)–O(1 W)	2.618(8)
Ce(1)–O(2 W)	2.557(8)
Ce(1)–O(34)#2	2.583(7)
Ce(1)–O(36)	2.403(6)
Ce(1)–O(39)	2.424(7)
Ce(1)–O(7)#1	2.510(5)
Ce(1)–O(8)	2.447(7)
P(1)–O(17)	1.549(7)
P(1)–O(28)	1.530(6)
P(1)–O(37)	1.531(7)
P(1)–O(6)	1.534(6)

Symmetry codes: #1 $-x+1, -y+1, -z+1$; #2 $-x, -y+1, -z+1$.

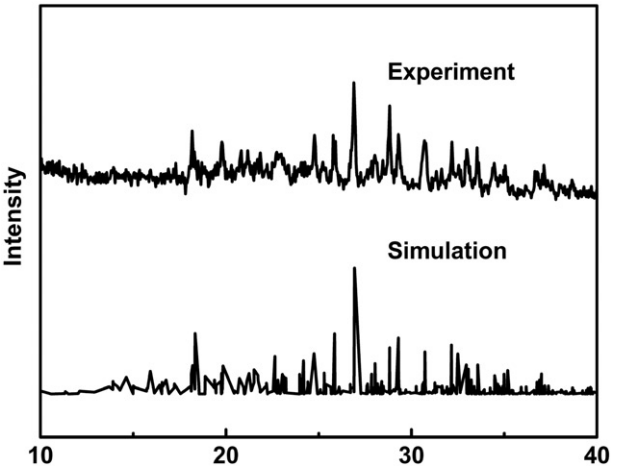

Figure 1. Comparison of the simulated and experimental XRPD patterns of **1**.

vacant site of $[\alpha\text{-}PW_{11}O_{39}]^{7-}$, coordinating eight oxygens in a bi-capped triangular prism environment. Therefore, adjacent molecular units of **1** are combined through the coordination of Ce1 to terminal O34A and O7B from the adjacent molecular units, generating a 1-D zigzag chain-like architecture (figure 2c). Similar 1-D zigzag chains have been observed in two silicotungstates $[Ce(\alpha\text{-}SiW_{11}O_{39})(H_2O)_3]$ [10] and $[Eu(\alpha\text{-}SiW_{11}O_{39})(H_2O)_2]$ [11].

The Ce1 with bi-capped triangular prism structure (figure 2b) has O8, O16, O36 and O39, O7B, O8, O39, and O34A, and O7B, O16, O36, and O34A atoms establishing the three side planes of the trigonal prism, and their average deviations are 0.0114, 0.1693, and 0.1111 Å, respectively. The distances between Ce1 and the three side planes are 1.2315, 0.6956, and 0.7406 Å, respectively. O1W and O2W occupy the two cap positions. The distance between O1W and the side plane defined by O7B, O8, O39, and O34A is 1.9168 Å and the distance between O2W and the side plane defined by O7B,

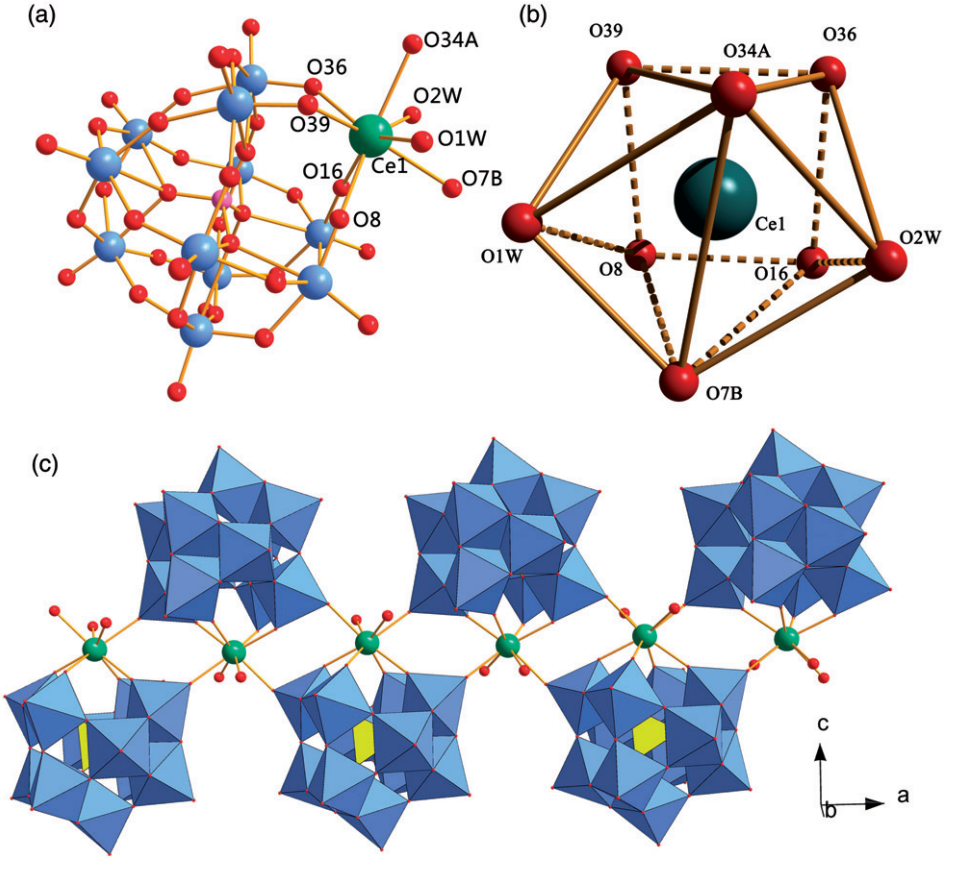

Figure 2. (a) Ball-and-stick representation of the asymmetric unit of **1**. (b) The bicapped trigonal prism geometry of the Ce(III) cation in **1**. Atoms with "A" and "B" in their labels are symmetrically generated (A: $-x, 1-y, 1-z$; B: $1-x, 1-y, 1-z$). (c) The 1-D zigzag chain-like arrangement of **1**. The $[(CH_3)_4N]^+$ cations and water molecules of crystallization are omitted for clarity.

O16, O36, and O34A is 1.8124 Å. The 1-D chains consist of monovacant Keggin-type POMs and lanthanide cations share similar coordination geometries: the lanthanide cation resides in the lacunary position of the polyanion, bound to two adjacent vacant polyanion subunits *via* two terminal oxygens. The average bond length between Ce and O is 2.492(20) Å, shorter than the distances of nine-coordinate Ce cations [10].

3.3. *IR and UV spectra*

The IR spectrum of **1** displays similar asymmetric vibrations to other Keggin-type polyoxoanion frameworks [12], in agreement with the results of X-ray diffraction structural analysis. In the low-wavenumber region, four characteristic vibrations centered at 980, 1079, 897, and 814 cm^{-1} are attributed to $\nu_{as}(W–O_t)$, $\nu_{as}(P–O_a)$, $\nu_{as}(W–O_b)$, and $\nu_{as}(W–O_c)$, respectively.

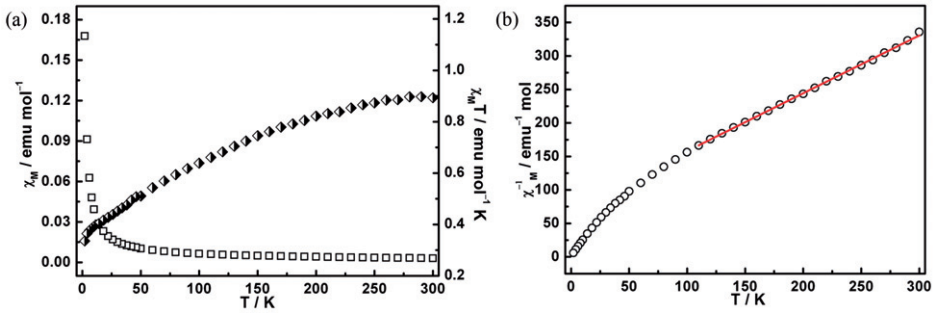

Figure 3. (a) Temperature dependence of $\chi_m T$ for **1** in the temperature range 2–300 K. (b) Temperature dependence of $1/\chi_m$ for **1** in the temperature range 2–300 K.

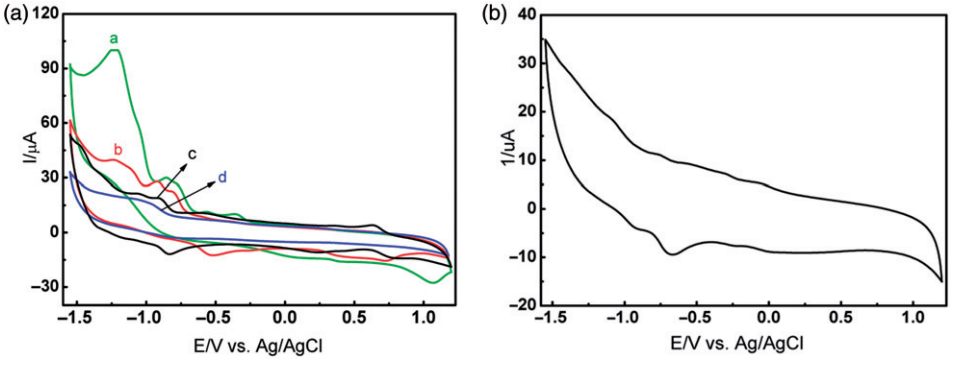

Figure 4. (a) Cyclic voltammograms of 0.5 mmol L^{-1} **1** in 0.5 mol L^{-1} Na_2SO_4 aqueous solution; curves: a, pH = 2.90; b, pH = 3.34; c, pH = 4.02; d, pH = 5.80. Scan rate: 50 mV s^{-1}. The pH value was adjusted with 0.1 mol L^{-1} H_2SO_4 and 0.1 mol L^{-1} NaOH aqueous solution, respectively. (b) Cyclic voltammograms of 0.5 mmol L^{-1} the compound α-$Na_7PW_{11}O_{39} \cdot nH_2O$ in 0.5 mol L^{-1} Na_2SO_4 aqueous solution; scan rate: 50 mV s^{-1}.

As depicted in figure 3, the UV spectrum shows two characteristic peaks in the range 190–400 nm: one strong absorption centered at 194 nm and one weak absorption centered at 251 nm. The former higher energy absorption can be assigned to pπ–dπ charge-transfer transitions of $O_d \rightarrow W$, whereas the latter lower energy absorption is attributed to pπ–dπ charge-transfer transitions of $O_{b,c} \rightarrow W$ bonds [13].

3.4. *Magnetic property*

The magnetic behavior of **1** is shown in figure 4(a) as the variation of $\chi_m T$ *versus* T plot, where χ_m is the corrected molar magnetic susceptibility. The observed value of $\chi_m T$ is 0.89 emu K mol^{-1} at room temperature, which is consistent with the theoretical value for one Ce(III) (0.8 emu K mol^{-1}). Upon cooling, the value of $\chi_m T$ decreases gradually and reaches a value of 0.34 emu K mol^{-1} at 2 K, indicating weak antiferromagnetic interactions between Ce^{III} ions and spin–orbital coupling interactions of the Ce^{III} ions. The curve of χ_m^{-1} *versus* T over the temperature range 168–300 K follows the

Curie–Weiss law with $C = 2.99\,\text{emu K mol}^{-1}$ and $\theta = -259.87\,\text{K}$, further confirming antiferromagnetic interaction and spin–orbit coupling interaction (figure 4b). However, the relation of χ_m^{-1} *versus* T between 168 and 2 K does not follow the Curie–Weiss law chiefly because the Kramers doublets of higher energy are successively depopulated as the temperature decreases.

3.5. *Thermal property*

The thermal property of **1** has been measured under flowing nitrogen with a heating rate of $10\,^{\circ}\text{C min}^{-1}$ from 25°C to 600°C (see online supplementary material). The TG curve exhibits two slow steps of weight loss: the first of 2.23% occurs between 25°C and 300°C, corresponding to the removal of two crystal water molecules and two coordination water molecules (Calcd 2.26%). The second weight loss of 9.33% (Calcd 9.31%) between 300°C and 600°C results from the loss of four tetramethylammonium groups.

3.6. *Electrochemical properties*

Electrochemical measurements of **1** ($0.5 \times 10^{-3}\,\text{mol L}^{-1}$) compared with the precursor $Na_7[\alpha\text{-}PW_{11}O_{39}]\cdot nH_2O$ were carried out in $0.5\,\text{mol L}^{-1}$ Na_2SO_4 aqueous solution by cyclic CV (see online supplementary material). All CV curves were recorded using Hg/Hg_2Cl_2 as the reference with a scan rate of $50\,\text{mV s}^{-1}$. The cyclic voltammogram for **1** (at pH = 4.02) exhibits two comparatively well-defined redox waves which are ascribed to W^{VI}/W^{V} [14] and Ce^{IV}/Ce^{III} [15] couples with midpoint peak potentials ($E_{p1/2}$) of −0.8697 and +0.6953 V, respectively. Obviously, the reduction peaks at −1.3140 and −1.0547 V attributed to redox processes of W^{VI}/W^{V} do not have the corresponding oxidation peaks [16]. The wave with $E_{p1/2} = +0.6953$ V in the positive potential range can be attributed to the reaction $[(\alpha\text{-}PW_{11}O_{39})Ce^{III}(H_2O)_2]^{4-} \leftrightarrow [(\alpha\text{-}PW_{11}O_{39})Ce^{IV}(H_2O)_2]^{3-} + e^-$ [15]. To highlight the influence of pH on the peak potentials in the cyclic voltammograms for **1**, the experiment was carried out in the above-mentioned media in wide pH regions. In the acidic direction, three redox peak potentials in the pH range of 4.0–5.8 become weaker, explained as the degeneration of the polyoxoanion fragment with increasing solution alkalinity [17]. In contrast, when pH is lower than 4.0, the reduction peak shape and number gradually strengthen or increase, while the oxidation peak shape and number gradually weaken or decrease; the peak position is shifted to the positive potential direction. This shows that redox processes become irreversible with the decreasing of solution pH, due to hydrogen evolution or framework change of the polyoxoanion fragment [18].

4. Conclusion

A cerium-substituted monovacant Keggin-type POM, with a 1-D zigzag chain built by $[(\alpha\text{-}PW_{11}O_{39})Ce(H_2O)_2]^{4-}$ moieties, has been synthesized in aqueous solution. The new complex was characterized by XRPD, single-crystal diffraction analysis, IR and UV spectra, magnetic, thermal analysis, and electrochemical behavior.

Magnetic measurement indicates that **1** exhibits spin–orbital coupling interactions and weak antiferromagnetic exchange. The electrochemistry of **1** reveals that the pH of the supporting electrolytic solution has a marked effect on electrochemical behavior. The synthesis and isolation of **1** provides useful information for exploring other monovacant Keggin-type POMs in aqueous solution.

Supplementary material

Supplementary material has been deposited with the Cambridge Crystallographic Data Centre (No. 679442; Fax: +44-1223-336033; E-mail: deposit@ccdc.cam.ac.uk).

Acknowledgments

This work was financially supported by the Natural Science Foundation of China, Special Research Fund for the Doctoral Program of Higher Education, Innovation Scientists and Technicians Troop Construction Projects of Henan Province, Natural Science Foundation of Henan Province.

References

[1] J.J. Borrás-Almenar, E. Coronade, A. Müller, M.T. Pope. *Polyoxometalate Molecular Science*, Kluwer Academic Publisher, Dordrecht, the Netherlands (2004).
[2] M.T. Pope. *Heteropoly and Isopoly Oxometalates*, Springer-Verlag, Berlin (1983).
[3] J.T. Rhule, C.L. Hill, D.A. Judd. *Chem. Rev.*, **98**, 327 (1998).
[4] A. Hiskia, A. Mylonas, E. Papaconstantinou. *Chem. Soc. Rev.*, **30**, 62 (2001).
[5] R.D. Peacock, T.J.R. Weakley. *J. Chem. Soc. A*, 1836 (1971).
[6] Z. Shi, L.R. Zhang, G.S. Zhu, G.Y. Yang, J. Hua, H. Ding, S.H. Feng. *Chem. Mater.*, **11**, 3565 (1999).
[7] A. Dolbecq, P. Mialane, L. Lisnard, J. Marrot, F. Sécheresse. *Chem. Eur. J.*, **9**, 2914 (2003).
[8] C. Brevard, R. Schimpf, G. Tourne, C.M. Tourne. *J. Am. Chem. Soc.*, **105**, 7059 (1983).
[9] G.M. Sheldrick. *SHELXS-97, Program for Crystal Structure Solution*, University of Göttingen, Göttingen, Germany (1997).
[10] M. Sadakane, M.H. Dickman, M.T. Pope. *Angew. Chem. Int. Ed. Engl.*, **39**, 2914 (2000).
[11] P. Mialane, L. Lisnard, A. Mallard, J. Marrot, E. Antic-Fidancev, P. Aschehoug, D. Vivien, F. Sécheresse. *Inorg. Chem.*, **42**, 2102 (2003).
[12] C. Rocchiccioli-Deltcheff, M. Fournier, R. Franck, R. Thouvenot. *Inorg. Chem.*, **22**, 207 (1983).
[13] J.Y. Niu, J.P. Wang. *Introduction of Heteropoly Compound*, Henan University Press, Kaifeng (2000).
[14] (a) I.M. Mbomekalle, B. Keita, M. Nierlich, U. Kortz, P. Berthet, L. Nadjo. *Inorg. Chem.*, **42**, 5143 (2003); (b) J.Y. Niu, J.W. Zhao, D.J. Guo, J.P. Wang. *J. Mol. Struct.*, **692**, 223 (2004); (c) J.P. Wang, J.W. Zhao, J.Y. Niu. *J. Mol. Struct.*, **697**, 191 (2004).
[15] N. Haraguchi, Y. Okaue, T. Isobe, Y. Matsuda. *Inorg. Chem.*, **33**, 1015 (1994).
[16] J.P. Wang, J.W. Zhao, P.T. Ma, J.C. Ma, L.P. Yang, Y. Bai, M.X. Li, J.Y. Niu. *Chem. Comm.*, 2362 (2009).
[17] J.Y. Niu, K.H. Wang, H.N. Chen, J.W. Zhao, P.T. Ma, J.P. Wang, M.X. Li, Y. Bai, D.B. Dang. *Cryst. Growth Des.*, **9**, 4362 (2009).
[18] J.Y. Niu, J.W. Zhao, J.P. Wang, P.T. Ma. *J. Mol. Struct.*, **699**, 85 (2004).